Responses to iron oxide and zinc oxide nanoparticles in echinoderm embryos and microalgae: uptake, growth, morphology, and transcriptomic analysis

Anne-Marie Geneviere, Evelyne Derelle, Marie-Line Escande, Nigel Grimsley, Christophe Klopp, Christine Ménager, Aude Michel, Hervé Moreau

Manuscript approved in Nanotoxicology:

Manuscript ID: INAN 1827074

RESPONSES TO IRON OXIDE AND ZINC OXIDE NANOPARTICLES IN ECHINODERM EMBRYOS AND MICROALGAE: UPTAKE, GROWTH, MORPHOLOGY AND TRANSCRIPTOMIC ANALYSIS.

Anne-Marie Geneviève*[#a], Evelyne Derelle[a,b], Marie-Line Escande[a],

Nigel Grimsley[a], Christophe Klopp[c], Christine Ménager[d], Aude Michel[d], Hervé Moreau [a]

[a]*Sorbonne Université, CNRS, Biologie Intégrative des Organismes Marins, BIOM, F-66650 Banyuls-sur-Mer, France*

[b]*Univ Brest, CNRS, IRD, Ifremer, LEMAR, F-29280 Plouzane, France*

[c]*INRA, Plateforme Bioinformatique Toulouse, Midi Pyrenees UBIA, Castanet Tolosan, France*

[d]*Sorbonne Université, CNRS, PHysico-chimie des Electrolytes et Nanosystèmes InterfaciauX, PHENIX, F-75005 Paris, France.*

[#]*After the first author, contributors are in alphabetical order*

**Corresponding author:* anne-marie.geneviere@obs-banyuls.fr, phone*: 33-4-68-88-7314 Observatoire Océanologique de Banyuls, BIOM-UMR7232, Avenue Pierre Fabre, F-66650 Banyuls-sur-Mer, France,*

RESPONSES TO IRON OXIDE AND ZINC OXIDE NANOPARTICLES IN ECHINODERM EMBRYOS AND MICROALGAE: UPTAKE, GROWTH, MORPHOLOGY AND TRANSCRIPTOMIC ANALYSIS.

Abstract :

We investigated the toxicity of Iron oxide and Zinc oxide engineered nanoparticles (ENPs) on *Paracentrotus lividus* sea urchin embryos and three species of microalgae. Morphological responses, internalization and potential impacts of Fe_2O_3 and ZnO ENPs on physiology and metabolism were assessed. Both types of ENPs affected *P. lividus* larval development, but ZnO ENPs had a much stronger effect. While growth of the alga *Micromonas commoda* was severely impaired by both ENPs, *Ostreococcus tauri* or *Nannochloris sp.* were unaffected. Transmission electron microscopy showed the internalization of ENPs in sea urchin embryonic cells while only nanoparticle interaction with external membranes was evidenced in microalgae, suggesting that marine organisms react in diverse ways to ENPs. Transcriptome-wide analysis in *P. lividus* and *M. commoda* showed that many different physiological pathways were affected, some of which were common to both species, giving insights about the mechanisms underpinning toxic responses.

Keywords: toxicity, marine organisms, metal oxide, transcriptomics

Introduction

Engineered nanoparticles (ENPs) have emerged as a new class of pollutants that may have toxic effects on ecosystems. A great variety of ENPs are now used in personal or health care products, paints, clothing, electronic devices and various other innovative goods. Consequently, ENPs are inevitably released to the environment, invading soils and waterways, through wastewater output or aerial dispersal, and ultimately reaching freshwater and marine ecosystems. According to the estimated global mass flow of ENPs from production to release (Keller and Lazareva 2014), metal oxide-ENPs (MO-ENPs) predominate in emissions to water, with titanium dioxide, zinc oxide, copper oxide, cerium dioxide and iron oxide ENPs being the most abundant discharged nanomaterials. On one hand, due to their unique properties Zinc oxide ENPs are one of the most widely used MO-ENPs. They are present in cosmetics, sunscreens and antifouling paints and are thus increasingly abundant in marine ecosystems (Ma *et al.* 2013, Baker *et al.* 2014). On the other hand, iron oxide ENPs have received increasing attention for biomedicine, biosensors (Magro *et al.* 2012, Marcus *et al.* 2016), and water treatments (Adeleye *et al.* 2016) leading to their consideration as emerging contaminants (Valdiglesias *et al.* 2016). Measurement of ENPs in natural conditions remains challenging and consequently there are only few data from the environment. Predicted environmental concentrations (PEC) have been estimated in freshwater from a few ng/L (Gottschalk *et al.* 2013, 2015, Lead *et al.* 2018) to 76 µg/L (Silva *et al.* 2011) for ZnO ENPs, in keeping with the measured concentration of 1.58 ± 0.59 µg/L in effluent water samples (Majedi *et al.* 2012). In seawater particulate concentrations of about 30 µg/L for Zn and 6 µg/L for Fe have been reported (Singhal *et al.* 2006).

Most ecotoxicological studies on MO-ENP impacts have been focused on freshwater species (Châtel and Mouneyrac 2017, Mukherjee and Acharya 2018), but biological effects in marine species are now also well documented (Baker *et al.* 2014, Canesi and Corsi 2016). In aquatic

media, the MO-ENP toxicity is highly dependent on the metal component: ZnO ENPs so far being most toxic (Mukherjee and Acharya 2018) while iron-based ENPs may be less harmful (Lewinski *et al.* 2008, Kadar *et al.* 2010). The biological activity of ENPs is also strongly related to their structure which depends on environmental conditions (Keller *et al.* 2010). Finally, toxicity is highly species-specific (Bondarenko *et al.* 2013, Exbrayat *et al.* 2015, Hou *et al.* 2018).

The fate and behaviour of MO-ENP in seawater are very different from those in freshwater. The higher alkalinity and ionic strength of the seawater as well as the presence of divalent cation and dissolved organic matter greatly influence suspended ENP structure (Blinova *et al.* 2010, Keller *et al.* 2010, Châtel and Mouneyrac 2017). Stronger aggregation or agglomeration of ENPs in seawater and a slow precipitation to the ocean floor affect ENP bioavailability. Another paradigm of ENP toxicity is the release of ions in the biological environment. Ion solubilization has been particularly well documented in the case of ZnO ENPs, where hydrated Zn^{2+} cations can form (Franklin *et al.* 2007, Xia *et al.* 2008, Ma *et al.* 2013), but the mechanism of ZnO ENP toxicity is still an ongoing debate (Bundschuh *et al.* 2018). ZnO ENP toxicity has been attributed to Zn ion leakage both in freshwater species (Heinlaan *et al.* 2008, Aruoja *et al.* 2009, Blinova *et al.* 2010, Miller *et al.* 2010) and in marine species (Miller *et al.* 2010, Wong *et al.* 2010, Fairbairn *et al.* 2011), but a recent report on marine clams has shown that ZnO ENP toxicity also depends on NP-specific features (Marisa *et al.* 2016). Moreover, the toxicity of ENPs on marine organisms is variable between taxonomic groups (Wong *et al.* 2010, Canesi and Corsi 2016, Mukherjee and Acharya 2018), but the molecular mechanisms which trigger the diversity of responses after exposure to ENPs remain largely unknown.

We compared two types of MO-ENPs known to be released in seawater, ZnO and γ-Fe_2O_3 (maghemite). To assess ENP toxicity, we chose two taxonomically distant species representing key groups in marine ecosystems, unicellular green microalgae (mamiellophycae) and

echinoderms (sea urchin), that have previously been used as models for ecotoxicological bioassays (Brayner *et al.* 2011, Fairbairn *et al.* 2011, Gambardella *et al.* 2016, Torres-Duarte *et al.* 2017). The physicochemical properties of ENPs were characterized before evaluating the responses of organisms after exposure to ENPs. ENP internalisation was evaluated using transmission electron microscopy (TEM) and transcriptomic analyses on whole organisms were designed to make an unbiased assessment of the molecular pathways affected.

Material and Methods

Preparation and characterization of metallic nanomaterials

Magnetic Nanoparticles of maghemite (γ-Fe_2O_3, mean size 10 nm) were synthetized according to the Massart's process (Massart 1981). $FeCl_2$ (177 g, 1.4 mol) and $FeCl_3$ (356 g, 2.2 mol) with HCl (37%, 100 mL, 12 mol) were co-precipitated by drop addition of NH_3 (22.5 %, 1 L, 11 mol) in distilled water. Magnetite (Fe_3O_4) nanoparticles formed were washed by magnetic decantation, dispersed in an acidic medium with HNO_3 (360 mL, 52.5 % in 2 L of distilled water) and oxidized in boiling $Fe(NO_3)_3$ (314 g, 1.3 mol). After a magnetic decantation and a second dispersion in diluted HNO_3, the magnetic nanoparticles of maghemite formed were washed three times in acetone and twice in ether. ENPs were then dispersed in water before coating with carboxymethyldextran (CMD). ZnO ENPs were synthetized as previously described (George *et al.* 2010), and were a generous gift of S. Pokhrel (Bremen University) (Fairbairn *et al.* 2011).

The ENPs dispersed in acidic media were coated with CMD (MW=15 000 $g.mol^{-1}$, [COOH] = 1.3 $mmol.g^{-1}$, Sigma-Aldrich, St Quentin Fallavier, France) following the method of Roger et al. (Roger *et al.* 1999) with an addition of CMD to the initial dispersion in a ratio [CMD]/[Metal] = 5%. They were finally ultra-filtered on MacroSep® 30 kDa twice for 15

minutes (Pall Life Sciences, VWR France, Fontenay-sous-Bois, France) and re-suspended in natural filtered (0.2 µm) sea water (NFSW). The sea water was collected offshore, 5 m deep, and analyzed by the SOMLIT platform: pH 8.27 $\pm$ 0.07, salinity: 38.01$\pm$ 0.1 g/L, POC 55.1 $\pm$ 14.3 µM.

The total metal concentration (mol/L) was determined by atomic absorption spectroscopy (AAS) with a Perkin-Elmer Analyst 100 apparatus after degradation of the ENPs in boiling HCl (35%). The ENP-CMD suspension at [Metal] = 5 10^{-2} mol/L was kept at 4 °C in the dark. ENP hydrodynamic diameters (Dh) were measured in NFSW through Dynamic Light Scattering using a Zetasizer Nano ZS (Malvern Instrument) operating at the scattering angle 174°. The collective diffusion coefficient D was determined from the second-order autocorrelation function of the scattered light. ENP Dh were calculated according to the Stokes-Einstein relation, $Dh = k_BT/3\pi\eta D$, where k_B is the Boltzmann constant, T the temperature (T = 298 K) and the solvent viscosity (η = 0.89 x 10^{-3} Pa.s for NFSW).

Handling of sea urchin gametes and embryo bioassay

Sea urchin *P. lividus* fertilized eggs were obtained as described in (Hanssen *et al.* 2012). Briefly, adults (about 7 cm in diameter) were collected in the Mediterranean Sea (Banyuls-sur-mer, France) and reared until use in filtered running sea water. Spawning was induced by intracoelomic injection of 0.2 M acetylcholine. Eggs were collected in NFSW, filtered through a 100 µm nylon sieve and washed three times with NFSW. For fertilization, sperm was diluted 10^5 fold in a 5% (v/v) egg suspension in NFSW. Only batches with at least 95% fertilized eggs were further used. One minute after fertilization, 500 µL of eggs (700 eggs/mL) were transferred to a 24-wells plate containing 500 µL of nanomaterial or metal ion solutions at different concentrations. Final concentrations ranged from 5 10^{-7} to 5 10^{-5} mol/L (from 2.8 10^{-5} to 2.8 10^{-3} g/L [Fe] and 3.2 10^{-5} to 3.2 10^{-3} g/L [Zn], 40 µg/L Fe_2O_3 or ZnO). The treatments

were applied post fertilization (p.f.) to avoid a possible interference with the fertilization process (Tualla and Bitacura 2016). Each concentration was tested twice per plate and NFSW were used as a control. All experiments were performed at 18 °C. The number of dividing cells was recorded after 80 min (when 100% of control cells was divided) and eggs were observed regularly with an inverted microscope (40X magnification) till the pluteus stage (48h). Each experiment was run in triplicate

Culture and treatment of algae

The three algal species *O. tauri* (RCC 4221), *M. commoda* (Noum17/RCC299) and *Nannochloris sp.*(sp. MBIC10596) were grown in enriched NFSW (L1 medium, Guillard and Hargraves 1993). Trace element solution and vitamins, purchased from Bigelow Laboratory (NCMA, USA) were diluted in NFSW and adjusted to pH 8. For culture growth and dose-response analyzes, algae were seeded at 5 10^6 cellules/mL in 20ml flasks and maintained at 20 °C under a 12/12 light/dark cycle (100 µmole photon/m^2s^{-1}). ENP were added 24h after seeding and each condition was run in triplicate. Every 24 hours over 13 days, 300 µL was sampled from each flask for cell counting. Sampled cells were preserved in 1% glutaraldehyde, frozen in liquid nitrogen and stored at -80°C until counting. Cell densities in defrosted samples were determined on a FACS Canto flow cytometer (Becton Dickinson, San Jose, CA, USA). Algae cells were counted according to their right-angle light scattering properties and their red fluorescence emission due to the chlorophyll A pigment (Trask *et al.* 1982). Accurate analyzed volumes and subsequent estimations of cell concentrations were calculated using Becton-Dickinson Trucount™ beads. Time course of culture growth were performed for Fe_2O_3 and ZnO ENPs concentrations ranging from 10^{-7} to 10^{-4} mol/L (from 5.6 10^{-6} to 5.6 10^{-3} g/L [Fe] and 6.5 10^{-6} to 6.5 10^{-3} g/L [Zn], 8 µg/L to 8 mg/L Fe_2O_3 or ZnO ENPs). Graphs of cell densities at 48h in response to increasing ENP concentrations were

plotted using a global nonlinear regression model based on sigmoidal curve and IC_{50} values were determined using Graph Pad Prism version 7.00 (GraphPad, San Diego, CA, USA).

Detection of ENPs by Transmission Electron Microscopy

Cultures of the three algal species were prepared for transmission electron microscopy (TEM) as previously described (Derelle *et al.* 2008). TEM images of ENPs dispersed in MOLA were recorded on a JEOL 2011 microscope working at 200 kV. The sea urchin embryos were fixed according to (Crawford and Burke 2004) using Millonig's phosphate-buffered glutaraldehyde. The cells were then embedded in Epon as previously.

Effect of ENPs on mRNA expression in Sea urchin, RNA-Seq transcript profiling

Gene expression was measured using RNAseq on pools of embryos collected at mid-gastrulae stage. Three fertilizations were independently performed with different male and female progenitors. The resulting three batches of fertilized eggs were divided in individual cultures containing either control NFSW, Fe_2O_3 ENPs or the corresponding ions, respectively Fe^{3+} ($FeCl_3$, $6H_2O$) or Zn^{2+} ($ZnSO_4$, $7H_2O$). About 3000 embryos were dispatched per well of 6-well plates, each containing 4 mL NFSW with or without nanomaterial or metallic ions at the above indicated concentrations and maintained at 18 °C until sampling. Embryos were harvested 24h p.f., briefly centrifuged and the resulting pellet of 2 wells (about 6000 embryos) were suspended in 200 µL Thioglycerol/homogeneization solution. RNA was extracted with Maxwell 16 LEV simply RNA kit (Promega) in Maxwell 16 instrument. Purified total RNA were collected in 50 µL RNase-free water and kept afterwards at -80 °C. RNA integrity (RIN) was estimated with a Bioanalyzer RNA 6000 nano and samples (RIN > 9) were send to Genewiz LLC (www.genewiz.com) for preparation of libraries and sequencing. Libraries were prepared via polyA selection and sequencing, 2 x 100bp paired-ends, was performed with HiSeq2500 (V4 chemistry).

In the Supplementary information S1, detailed protocols are reported on RNA-Seq analysis, mapping of sequenced reads and differential expression analysis. Briefly, the read quality of the RNA-Seq libraries was evaluated, a *de novo* transcriptome was assembled and annotated by BLAST comparison both with the genome sequences of closely related species, *Strongylocentrotus purpuratus and Ciona intestinalis* or with RefSeq (NCBI). Reads were realigned back to contigs and the contig expression counts were generated. Analysis of differentially expressed (DE) genes and data visualizations were performed in the R statistical environment (https://www.r-project.org/). DE genes were identified using R package edgeR (Robinson *et al.* 2010) with normalization for RNA composition and pairwise comparisons using the general linearized model likelihood ratio test. Contigs were accepted as significantly DE with a threshold of 1% as the false discovery rate (FDR) and when logCPM>0 and log2-fold-change (|LFC|) > 1. DE contigs were identified as enriched in Gene Ontology (GO) terms and metabolic pathways by searching against the GO and the KEGG databases (Ashburner *et al.* 2000, Kanehisa *et al.* 2006, 2008). For further comparisons, Venn diagrams were made with jvenn (http://jvenn.toulouse.inra.fr/app/example.html) (Bardou *et al.* 2014) to obtain the number of significantly expressed genes, which were shared among groups or unique in each experimental condition.

Effect of ENPs on mRNA expression in the microalga M. commoda, RNA-Seq profiling

Three independent cultures of *M. commoda* (Noum17/RCC299) were grown as described above. Flasks containing 140 mL were prepared from those cell cultures in early exponential phase and ENPs or the corresponding metal ions were added 24 h later. For RNA extraction, 100 mL of culture were sampled per vial 48 h later and the *M. commoda* cells were harvested by centrifugation at 8,000 *g* for 20 min at 4°C. The pellets were then flash frozen in liquid

nitrogen and stored at -80°C. Total RNA was extracted using Maxwell 16 LEV simplyRNA purification kit (Promega) in the Maxwell instrument and RNA concentration and integrity was estimated using the Bioanalyzer RNA 6000 nano (RIN>9). Selection for polyadenylated RNA, library preparation and sequencing was performed by the GeT-PlaGe GenToul platform (INRA, France). Fifteen RNA libraries were prepared using Illumina TruSeq Stranded mRNA kit. RNA libraries were sequenced on the Illumina Hi-Seq 3000 platform on 2 lines generating paired end reads of 150 bp in length with a total of 30 million reads per sample. Bioinformatic analysis of transcriptomes is detailed in Supplementary information S2. Briefly, RNA-Seq reads were mapped on the reference *M. commoda* genome available in the JGI database (https://genome.jgi.doe.gov/pages/search-for-genes.jsf?organism=MicpuN3v2) (Worden *et al.* 2009) and the transcripts were quantified as TPM. Analysis of DE genes was performed as described above.

Results

Physico-chemical characterization of nanomaterials

ENPs were coated after their synthesis with CMD. Due to COO^- groups, a metal-ion complex formed at the oxide (ZnO or Fe_2O_3) surface allowing the stabilization of the particles by steric repulsion even in highly salty solutions like sea water. The mean physical diameter of coated ENPs observed in TEM was 10 nm (Figure 1A-B), equal to the initial ENP size, thus the coating did not change their mean diameter. To evaluate the ENP aggregation state in culture conditions, natural seawater for sea urchin embryos or seawater-based L1 medium for algal culture, the hydrodynamic diameter D_h, i.e. the physical diameter with its solvation layer, was measured. Immediately after their dispersion in NFSW at 20 °C, D_h for Fe_2O_3 ENPs was 70 nm, instead of 33 nm in distilled water (Bachelet-Violette *et al.* 2014), and 90 nm for ZnO ENPs. Fe_2O_3 ENPs displayed a slight negative charge with a zeta potential of -7 mV. D_h

increased afterwards very rapidly with time until a threshold corresponding to the sedimentation point (6h, 1448 nm) (Figure 1C). Without CMD, ENP precipitation was immediate (data not shown), thus the coating helped to maintain the ENPs in suspension for longer during the toxicity experiments. When measured just after dispersion in NFSW-based L1 medium, D_h for Fe_2O_3 ENPs was 39.2 nm with a zeta potential of -6 mV. A further characterization by TEM of Fe_2O_3 ENP behaviour over 48h in L1 medium showed the presence of large aggregates of ENPs but no morphological change of nanoparticles indicating that they are not degraded (Figure 1D-F). Stock suspensions of coated ENPs were further diluted in NFSW or L1 medium just before use in the bioassays. Our rationale was to find experimental conditions that lead to assessable alterations of the selected physiological endpoints in bioassays to permit insights to be gained about the mechanisms induced by exposure to ENPs. Finally, the range of concentrations retained for bioassays were 10^{-7} to 10^{-4} mol/L for [Fe] or [Zn] (8 µg/L to 8 mg/L Fe_2O_3 ENP and 8.1 µg/L to 8.1 mg/L ZnO ENP), which include the reported values of PEC.

Sea urchin embryotoxicity

Sea urchin *P. lividus* embryos were exposed to ZnO or Fe_2O_3 ENPs, and their corresponding metal ions, during a 48h developmental time course (Figure 2). Malformations in embryos were classified according to Carballeira et al. (Carballeira *et al.* 2012), compared to embryos developing in control conditions (NFSW). Abnormalities extended from incorrect location of skeletal rods to developmental blocks, depending on the treatment. Zn-containing chemicals, either ENPs or soluble $ZnSO_4$, were toxic to developing embryos, with a higher toxicity of the ionic form Zn^{2+} (Figure 2F). Larvae with cross or non-joining tips of skeletal rods or deformed arms were observed at lower concentrations, while gastrulation was altered with severe impairment of spicules elongation at concentrations of 10-5 mol/L [Zn] of ZnO ENPs (6,5 10^{-4} g/L) and above (Figure 2D). In contrast, Fe_2O_3 ENPs did not induce major developmental

delay or severe abnormal morphologies (Figure 2B). However, a significant heterogeneity in the size of the treated larvae at the pluteus stage was observed (Figure S1). Fe^{3+} did not alter embryo development (Figure 2C).

We then investigated by TEM whether the limited toxic effect of Fe_2O_3 ENPs could be attributed to a lack of penetration in embryos. Figure 3 shows the internalization of ENPs which accumulate in cytoplasmic vesicles of ectodermal cells or in vesicles bordering the outer cell membrane. Elemental analysis confirmed the particle identity with sizes of about 10 nm in diameter (Figure 3D). Fertilization membrane removal before ENP addition did not change ENPs localization even if a slightly higher density of ENPs-containing vesicles was observed (data not shown).

Effects of ENPs on gene expression in sea urchin embryos

Sea urchin fertilized eggs were exposed for 24h to Fe_2O_3 and ZnO ENPs concentrations which produced morphological alterations from gastrula onward (5.0 10^{-5} mol/L [Fe], 10^{-5} mol/L [Zn]) or to an equivalent ionic concentration of soluble metal. Using Illumina RNA-Seq, a mean of 8,5 10^7 read pairs were obtained from control and treated samples (GEO-GSE1404). The number of sequences in cDNA libraries ranged from 25 to 34 million (100bp) read pairs. The *de novo* transcriptome was assembled leading to 63389 contigs. Quantitative data on the comparative transcriptome analysis are summarized in Supplementary data files S1 (up-regulated contigs) and S2 (down-regulated contigs). The number of DE genes in response to metal exposure are reported in Table 1 and visualized as Venn diagrams in Figure 4.

Table 1 position

Only few predicted contigs were DE after Fe_2O_3 ENPs or $FeCl_3$ exposure with the applied criteria. This result was concordant with the weak morphological effect observed in presence

of iron. Only one contig (Sina_LOC587958.3.3), predicted as the zinc transporter ZIP12, was up-regulated in response to Fe_2O_3 ENPs. This gene was not altered by $FeCl_3$ but highly down-regulated (|LFC|>3) in response to Zn, either as ENPs or ion. The remaining three Fe_2O_3 ENP DE contigs were down-regulated, one of them (Sina_LOC577189.1.2, an endoglucanase) being repressed regardless of the treatment. In contrast, a much larger set of contigs were DE when embryos were challenged with ZnO ENPs and to an even greater amount in response to $ZnSO_4$ treatment.

To highlight the more important biological processes (BP) or molecular functions (MF) participating in the ENP response, a GO analysis was performed (Figure S2). This analysis revealed that the processes most affected both among the up-regulated and the down-regulated contigs were related to "transcription regulation". The fraction of genes involved in "metallo-endopeptidase activity" was also enriched among the up-regulated contigs. Despite having a lower p-value, these GO terms were also enriched upon $ZnSO_4$ treatment.

Among the 196 DE contigs highly up-regulated (LFC>3) after ZnO ENP exposure, 23 encoded proteins of the metallothionein (MT) family (w/o an assigned GO term), all of them being more severely induced upon $ZnSO_4$ exposure (Figure S3). Seven were also up-regulated, though more weakly, in the presence of $FeCl_3$ while none of them were stimulated by Fe_2O_3 ENPs. A notable effect was also observed for three contigs encoding metalloendopeptidases, *MMP16* precursor, *BP10* and a type IV collagenase, which are highly induced in response to zinc, either as ENP or ionic. Nine other Zn-dependent contigs encoding metalloendopeptidases were also induced, less severely, in response to both forms of zinc metal.

Among the highly up-regulated contigs responding to ZnO ENPs, 17 were related to the enriched BP-transcription regulation GO terms. Several of these genes belong to the signalling pathways that specify cell fate along the sea urchin developmental axes such as *FoxQ2, Admp1 and 2, Unc4* or *Lefty* (Figure S4). Other components of the gene regulatory networks (GRNs)

which control development patterning, although not classified under this GO group, were highly down-regulated, including genes such as *ankAT-1, dkk3 or sfrp5*. Moreover, in agreement with the complete inhibition of spicule growth when embryos were challenged with ZnO ENPs, the expression of the spicule matrix gene *SM30* was found to be repressed in response to ZnO ENPs and $ZnSO_4$. This inhibition was confirmed by qPCR (data not shown). The BP-GO "transmembrane transport" type of functions were also enriched. These included predicted Zn transporters of the ZIP family, ZIP 10 and 12, ZIP12 being more highly down-regulated by ZnO ENPs and Zn^{2+} while up-regulated by Fe_2O_3 ENPs, as mentioned above and not affected by Fe^{3+}. In addition, MF-GO terms related to "Acetyl-CoA or biotin carboxylase activities" were also enriched among the highly down-regulated contigs. A KEGG analysis of these contigs showed that the encoded ACAC.1.3, 2.3 and 3.3 proteins belong to the AMPK signalling pathway which affects fatty acid biosynthesis. The enriched cholinesterase activity GO term includes the Cholinesterase 1 and 2 encoding contigs, the second one being highly down-regulated. Many of the contigs that were highly regulated in response to ZnO ENPs were also highly affected after exposure to $ZnSO_4$, however our analysis also revealed DE contigs specifically responding to ZnO ENPs but not to $ZnSO_4$ (Figure 4). Twenty-nine contigs in the latter group were highly stimulated, including a multidrug and toxin extrusion protein (Sina_LOC100891823) and a tubulin alpha-1 chain (TBA1.1.12), while 53 genes were highly repressed, most of them encoding uncharacterized proteins.

Culture growth responses of microalgae

Iron and zinc ENP toxicity was tested on three strains of picophytoplankton, *O. tauri* and *M. commoda* (both of the Mamiellophyceae class) and *Nannochloris sp* (class Trebouxiophyceae). Growth of *O. tauri* and *Nannochloris* were unaffected by the presence of ENPs in the culture medium (data not shown). In contrast, when *M. commoda* cultures were exposed to iron or zinc

ENPs, their exponential growth stopped rapidly and in a dose-dependent way (Figure 5). IC50 measurement at 48h showed that this algal strain is more sensitive to ZnO ENPs (IC50 = 4.35 10^{-6} mol/L, with a 95% confidence interval (CI): 3.55 to 5.37 10^{-6} mol/L) than Fe_2O_3 ENPs (IC50 = 3.19 10^{-5} mol/L with 95% CI: 2.72 to 3.93 10^{-5} mol/L).

To investigate if Fe_2O_3 ENPs penetrate the algal cells as they do in sea urchin embryonic cells, ENP-treated *O. tauri* and *M. commoda* algae were examined by TEM 48h after addition of ENPs. We observed neither internalization nor morphological perturbation of *O. tauri* cells, in agreement with the lack of cell growth inhibition. In contrast, *M. commoda* cell morphology was severely perturbed and we rarely observed intact flagella (Figure 6). ENPs were never visualized inside the cells without simultaneous membrane degradation and cell lysis. Fe_2O_3 ENP aggregates were often seen in close contact with the outer membrane (Figure 6 C,D) of cells with damaged envelope. In addition, depending on the species of alga the abundance of Fe_2O_3 ENP aggregates in the medium varied, with larger and more abundant aggregates for *O. tauri* and *Nannochloris* than for *M. commoda* (Figure S5).

M. commoda transcriptomic response to ENP exposure

We used RNA-Seq to compare gene expression patterns of the ENP-sensitive algae *M. commoda* cultured with or without metal oxide ENPs. Concentrations of ENPs were chosen from the growth profile described above to produce 60 to 80% growth inhibition of cultured cells: 3 10^{-5} mol/L [Fe] for Fe_2O_3 ENPs and 10^{-5} mol/L [Zn] for ZnO ENPs. Parallel cultures were treated with an equivalent ionic concentration of Fe^{3+} or Zn^{2+}. *M. commoda* cells were collected 48h after addition of the chemical compounds, when control cultures were still growing exponentially. For each sample, a fraction of the cell culture was harvested and total RNA was extracted, the growth rate of remaining cells being surveyed till day 10 (Figure S6). Only the ENP form of the metal oxides altered the growth rate of the *M. commoda* cultures.

RNAs were processed for preparation of libraries and further Illumina sequencing (NCBI-GEO-GSE140694). The RNA-Seq reads for each sample, mapped back to the *M. commoda* genome sequence, were used to calculate the expression level of unigenes and analyse the DE genes (Supplementary data, files S3 and S4). The numbers of DE genes for each comparison are summarized in Table 2 and visualized as Venn diagrams in Figure 7.

Table 2 position

The impact of $FeCl_3$ was very weak (only 0,3% of DE genes with |LFC|>3) and similarly, very few genes were highly repressed (0,7%) in response to $ZnSO_4$, but a higher proportion of them was induced. The slightly more pronounced response to Zn^{2+} compared to Fe^{3+}, with a higher proportion of up-regulated than down-regulated genes, matched with the observed small delay in the growth profile at 48h post Zn^{2+} addition.

Of the 918 DE genes specific to ENPs (common to Fe_2O_3 and ZnO, not responding to ions), 7 (0,2%) were highly induced, with 3 having a predicted annotation: *SfsA*, a transcription factor involved in maltose metabolism, *MFS1*, a transporter of the Major Facilitator Superfamily and *RCC1* a Regulator of Chromosome Condensation (Figure S7). Only one gene, *MDH5,* orthologous of the *C. reinhardtii* NADP-dependent malate dehydrogenase (EC 1.1.1.37) was highly repressed. In addition, the *hsp90* genes encoding stress chaperone proteins were either specifically altered or more intensively altered by ENPs than their corresponding ions while ENPs specifically induced *hsp20* expression. Two essential cell cycle genes were also preferentially repressed in response to ENPs, albeit to a lesser extent (lower LFC), *CDKD,* the CDK activating kinase, and *APC3* a subunit of the Anaphase Promoting Complex (Figure S7). Among the genes up-regulated in response to ENP exposure, the GO terms linked to the BP-microtubule-based movement predominated (Figure S8). Several transcripts in this GO group were highly induced in response to both ENPs as well as Zn^{2+} ions, but not induced or to a lower extent by Fe^{3+} ions (Figure S7), for example the gene encoding dynein heavy chain,

DHC6, involved in the movement of flagella (Mitchell 2007), and the CDHC1B gene or PKD2, a member of the TRP family of Ca^{2+}-permeable nonselective cation channels (Tsiokas 2009) which participates in intra-flagellar transport and calcium signaling in Chlamydomonas (Huang et al. 2007).

Among the down-regulated genes, "translation" was the main biological process altered by ENPs and Zn^{2+}, associated to the over-representation of genes linked to the MF "structural constituent of ribosome" and "translation initiation" (Figure S8). Several genes relevant to these GO terms were highly down-regulated (|LFC|>3) upon ENPs exposure, i.e. the ribosomal protein L1, the Lysyl-tRNA synthetase and the eIF4-gamma/eIF5/eIF2-epsilon described gene, but none gene of these groups was notably repressed by the corresponding ions. In addition, several genes related to nitrogen transport, either ammonium transporters (AMT) or nitrate transporters (NRT), were strongly down-regulated by both ENPs (Figure S7) but only changed weakly by the metal ions.

Discussion

We investigated the toxicity of two types of MO-ENPs (Fe_2O_3 and ZnO) on two different marine taxonomic groups, echinoderms and micro-algae. To our knowledge, this is the first report using a global gene expression approach to survey the molecular mechanisms affected by exposure to MO-ENPs in these marine organisms, and it provides new insight about MO ENP toxicity.

Upon dispersion in NFSW or algal culture media, ENPs rapidly formed aggregates as evidenced by Dh increase (Figure 1C). Moreover, visualization by TEM showed that this tendency to form aggregates varied in L1 algal media according to the species in culture (Figure S5). This shows that not only the SW ionic strength and organic matter content affect the ENP aggregation kinetics and settling rates (reviewed in Lead *et al.* 2018) but also that the interactions with organisms may influence ENP structure and in turn alter the ENP bioavailability and toxicity.

Mode of interaction and biological response in sea urchin embryos

TEM analysis showed that Fe_2O_3 ENPs penetrated the fertilization envelope and the plasma membrane of ectodermal cells of the sea urchin embryos, accumulating in cytoplasmic vesicles (Figure 3). This translocation through the plasma membrane probably occurs by endocytosis due to the high level of this kind of trafficking during early sea urchin development (Covian-Nares et al. 2008, Wu et al. 2015). Internalization of silver as well as copper or zinc oxide ENPs was already observed in different species of sea urchin embryos (Piticharoenphun et al. 2012, Wu et al. 2015, Torres-Duarte et al. 2016). In mammalian cells, CMD-coated maghemite ENPs were shown to be stored in lysosomes (Levy et al. 2011, Satori et al. 2011) where they are expected to be degraded under acidic conditions. Such ENP sequestration, in endosomes or lysosomes, given the harmelessness of the iron ionic form (Fe^{3+}), probably explains the low toxic effect observed in sea urchin embryos. Conversely, both ZnO ENPs and $ZnSO_4$ were highly toxic for these embryos (Figure 2). (Fairbairn *et al.* 2011) attributed the toxicity of non-coated ZnO ENPs on sea urchin embryos mainly to soluble Zn^{2+}. However, using CMD-coated ZnO ENPs, we found that only 6% of the Zn content was solubilized in 24 hours (data not shown). Nevertheless, strong morphological alterations were observed in embryos. This suggests that toxicity of ZnO ENPs was only partly related to their solubility, the action of other ENPs physicochemical characteristics being also important for the resulting toxic effect, as already reported in sea urchin and other marine organisms (Wong et al. 2010, Manzo et al. 2013, Zhao et al. 2013, Yung et al. 2015, Kim et al. 2017, Oliviero et al. 2017). The transcriptomic analysis identified overlap in the responses to ionic and NP forms of zinc in *P. lividus* with often stronger perturbation of the gene expression for the ionic form (higher LFC). However, marked differences were also found in the elicited BP indicating a distinct effect of the particulate form compared to the ionic one. Nevertheless, no one gene was specifically

altered by both iron-and zinc-based ENPs in sea urchin, probably because the surface properties of ENPs are unique to each MO.

The global gene expression analysis in response to ZnO ENP exposure revealed changes in various cell mechanisms including a repression of metal uptake, a strong induction of metal binding proteins, an alteration of detoxification processes and a severe repression of genes which regulate developmental patterning of sea urchin embryos.

To cope with external zinc excess, genes encoding proteins of the ZIP family, which facilitate zinc/iron uptake to the cytosol and regulate gene homeostasis (Baltaci and Yuce 2018), were repressed. In contrast, the expression of the heavy metal binding MT were massively induced. MT induction was a common response upon exposure to the ionic form of zinc, cadmium or manganese in sea urchin embryos (Roccheri *et al.* 2004, Migliaccio *et al.* 2014, Ragusa *et al.* 2017) but also to ZnO ENP in nematode (Ma *et al.* 2009, Polak *et al.* 2014). In addition to be the main metal-responsive genes in many systems, MT are also sensitive to oxidative stressors or irradiation (Russo et al. 2014), since they participate in scavenging of the reactive oxygen species (*ROS)*. Induction of ROS and the resulting oxidative stress is the most commonly reported mechanism of nanotoxicity (Al-Subiai *et al.* 2012, Rocha *et al.* 2015, Marisa *et al.* 2016). In sea urchin embryos, NADPH-oxidase (Nox) induction evokes the production of ROS, but superoxide dismutase (SOD) or catalase (CAT) stimulation were not observed, suggesting that ROS scavenging could be ensured mainly by the MT redox cycle rather than the glutathione redox complex. On the other hand, the detoxification processes were disrupted: a predicted Cytochrome P450 (Phase I detoxification process) was repressed and gluthatione S-transferase (GST) encoding genes (Phase II) were either stimulated (GST- Ω and GST- θ) *or* inhibited (*GST-α)*. In addition, the genes encoding the Multidrug Resistance-associated Proteins (MRP) were repressed. These ABC-transporter proteins, which normally protect embryos against

xenobiotics, were already shown to be inhibited by Zn and Cu ENPs and to be responsible for a chemosensitizer effect of ENPs in sea urchin embryos (Wu *et al.* 2015).

Despite the stimulation of defence mechanisms, strong alterations of embryos development were induced by ZnO ENPs treatment. The morphological alterations were visible from gastrula onward. The lack of alteration of cleavage stages demonstrated that cell division itself was not affected and accordingly the expression of cell cycle-related genes was not modified. In contrast, ZnO ENPs mainly perturbed the "DNA-dependent transcriptional regulatory processes" (Figure S2), which are only required in sea-urchin for post-blastula development. Similarly, microarray data showed that Ag nanotube exposure led to down-regulation of numerous genes related to DNA-dependent transcriptional regulation in zebrafish embryos (Park and Yeo 2015). Most of these repressed genes, as well as those related to the over-represented "growth processes", are part of the signalling pathways that specify cell fate along the sea urchin developmental axes: *foxQ2*, *AnkAT-1, sfrp5* and *dkk3, admp1 and 2, Lefty,etc.* (Figure S5). Their down-regulation is well correlated with the observed failure in gut and skeleton formation (Fig. 2D) as detailed in Supplementary information S3. The disruption of genes involved in the TGF-ß signalling pathway, which regulate skeletal morphogenesis (Sun and Ettensohn 2017), may explain the consecutive down-regulation of *SM30*, a marker of skeletal development which was already shown to be repressed in response to Cd (Marrone *et al.* 2012, Migliaccio *et al.* 2014). Trans-membrane transport processes and in particular Ca^{2+} transport are also over-represented in down-regulated genes. This alteration may participate, in addition to *SM30* repression, to a biocalcification defect leading to skeleton disruption. In addition, disruption of calcium homeostasis during early developmental stages, as well as generation of ROS, are known to disturb the establishment of embryo axes (Akasaka *et al.* 1997, Coffman and Davidson 2001).

Mode of interaction and biological response in microalgae

Growth of *M. commoda* was inhibited by both ENP types whereas *O. tauri* and *Nannochloris* were unaffected. In the corresponding microalgal culture media, the ENP aggregation propensity was negatively correlated with the observed toxicity. The extracellular polymeric substances (EPS) secreted by algae are known to enhance the aggregation of ENPs, limiting their interaction with the microalgae surface and the ENP toxic abilities (Quigg *et al.* 2013, Chiu *et al.* 2017, Morelli *et al.* 2018, Chen *et al.* 2019). In the *M. commoda* transcriptomic analysis, we noted that the *AMYA1* ∝-amylase encoding gene which belongs to the starch and sucrose metabolic pathway (map 00500, Figure S9) was strongly induced by ENPs (LFC>3), supporting the hypothesis of a stimulation of the carbohydrate metabolism also in this species. While this stimulation was not sufficient to shape a protective bio-barrier in *M. commoda*, a higher EPS secretion in *O. tauri* and *Nannochloris* could explain a decreased bioavailability and a reduced toxicity in these two species.

In *M. commoda,* ENPs, but not the metal ionic forms, strongly inhibited growth. The analysis of DE genes showed that two zinc/iron permeases of the ZIP family were specifically repressed by ENP, suggesting a response to cope with metal ion excess. ENPs were never observed by TEM inside cells of this alga, which does not possess cell wall. In contrast, ENP aggregates were found in close contact with the external membrane of lysing cells (Figure 6) suggesting that damage to the cell membrane is a critical step of cytotoxicity.

The gene expression analysis showed that oxidative stress mechanisms were activated upon exposure to both kinds of ENPs. Genes responsive to ROS production, such as Cu-Zn *SOD3* superoxide dismutase, ODA-LC 3 or 5 thioredoxin family members and CCP1 peroxidase were induced. A large number of studies indicate that oxidative stress is the dominant toxicity mechanism of ENPs on algae (von Moos and Slaveykova 2014) and that ROS exceeding the scavenging capacity of antioxidative enzymes would directly damage the cell membrane (Chen *et al.* 2019). In contrast to sea urchin, scavenging proteins of the MT family were poorly

induced in *M. commoda* (wlab. 246805.1) or even repressed (wlab.240127.1). In contrast, MDH5, a chloroplast-localized protein which contributes to avoiding radical formation, was found highly and specifically induced by ENP exposure (Scheibe 2004). Moreover, we noted an over-representation of the up-regulated genes related to photosynthesis light harvesting (LH) processes and in particular the ENP-specific up-regulation of *LHCSR2* and several members of the *CBR/ELIP* family. This family of light-harvesting-related proteins is not only induced in response to photo-oxidative stress (Montané and Kloppstech 2000, Cuvelier *et al.* 2017) but are also responsive to other types of stress in plants, including cold stress (Montané *et al.* 1999). Their stimulation after ENP exposure is, as far as we know, the first reported response to a physico-chemical stress in algae. Another sign of ENP-induced stress in this algae is the specific induction of isoforms of *hsp20* by both ENPs (Supplementary data file S3). In addition, expression of genes involved in the detoxifying mechanisms such as *GST2*, *CYP97C* of the cytochrome P450 family and two members of the ATP-binding cassette efflux transporters (ABC) were specifically repressed by ENPs.

The biological processes related to microtubule-based movement are preferentially represented among the up-regulated transcripts in response to ENPs (Figure S8). Among the up-regulated transcripts relevant to this pathway are the dynein DHC6 and the cation channel PKD2, both involved in the movement of the flagellum (Huang *et al.* 2007). These changes might be the cause of the flagellar damage observed in the cultures. A loss of flagella was also observed in the microalga *D. viridis* after exposure to cerium oxide ENP (Klimova *et al.* 2019). Conversely, the most abundant groups of down-regulated transcripts consisted of genes involved in translation, suggesting a decrease in the protein content or the production of misfolded proteins. A similar severe alteration of translation was observed in *Arabidopsis thaliana*, in bacteria treated with ZnO ENP (Landa *et al.* 2012, Su *et al.* 2015), in the fresh water phytoplankton cyanobacterium *Microcystis aeruginosa* exposed to silver ENPs (Qian *et al.* 2016) or in

copepods challenged with nickel ENPs (Zhou *et al.* 2018). Finally, essential cell cycle genes (CDKD, APC3), were specifically repressed by ENPs, probably a critical step in *M. commoda* growth inhibition.

Conclusion

This analysis confirmed that marine organisms respond in a highly variable way to ENPs. TEM revealed that ENPs penetrated sea urchin embryos, where they accumulate in cell vesicles, presumably endosomes or lysosomes. In contrast, ENPs were not internalized by the tested microalgal cells, but interacted closely with the external cell surface inducing pronounced damage to the plasma membrane and cell lysis. The induced biological responses were also distinct: while sea urchin embryos were sensitive (to different extents) to both ENPs, microalgae responded in a highly species-dependent manner; growth of *M. commoda* was inhibited by both ENP types whereas *O. tauri* and *Nannochloris* were unaffected. Notably, in *M. commoda* only the ENP forms of Fe and Zn were toxic, while in sea urchin the ionic form of zinc produced morphological alterations at lower [Zn] than the ENP form. However, in both echinoderm and algae, zinc-based ENPs had a higher toxicity than iron ENPs, though growth of *M. commoda* was severely inhibited by Fe_2O_3 ENPs.

The transcriptomic analysis confirms that the outcomes of MO ENP exposure differ according to the metal oxide and the species. However, in both kinds of reactive organisms, responses linked to the nanoparticular structure were evidenced. Indeed, MO ENPs and their corresponding ions elicited different patterns of gene expression in both model organisms. ENPs induce alterations of some common molecular mechanisms in both organisms, such as in the transmembrane transport, which ensures metal homeostasis, the detoxifying mechanisms, and the Ca^{2+} transport or calcium signalling pathways. The response to oxidative stress is also observed in both species but the respective involvement of detoxifying and redox responses

differ according to the species. Moreover, potential biomarkers of ENP exposure have been identified and should be confirmed by further experiments.

Acknowledgements,

The authors would like to dedicate this publication to Dr. Hervé Moreau who died unexpectedly during the revision of this article.

The authors thank Dr. Pascal Giraud and the ORDECO organization (https://www.ordeco.org/) for fruitful discussions and assistance during the project, Christophe Salmeron (SU/CNRS BioPIC Imaging and OOB Cytometry platform) for cytometry analysis, Elodie Desgranges (OOB-UMR7232) for technical assistance in microalgae culture, and the microscopy platform of the Institut des Matériaux de Paris Centre **(**IMPC) - Fédération de Recherche 2482.

Funding

The authors thank the CNRS (Missions pour les initiatives transverses et interdisciplinaires) and EMBRC.France for financial support.

Supplementary information

Supplementary information to this article is available online

Declaration of interest statement

The authors declare that there is no conflict of interest regarding the publication of this article.

References

Adeleye, A.S., Conway, J.R., Garner, K., Huang, Y., Su, Y., and Keller, A.A., 2016. Engineered nanomaterials for water treatment and remediation: Costs, benefits, and applicability. *Chemical Engineering Journal*, 286, 640–662.

Akasaka, K., Uemoto, H., Wilt, F., Mitsunaga-Nakatsubo, K., and Shimada, H., 1997. Oral—aboral ectoderm differentiation of sea urchin embryos is disrupted in response to calcium ionophore. *Development, Growth & Differentiation*, 39 (3), 373–379.

Al-Subiai, S.N., Arlt, V.M., Frickers, P.E., Readman, J.W., Stolpe, B., Lead, J.R., Moody, A.J., and Jha, A.N., 2012. Merging nano-genotoxicology with eco-genotoxicology: An integrated approach to determine interactive genotoxic and sub-lethal toxic effects of C60 fullerenes and fluoranthene in marine mussels, Mytilus sp. *Mutation Research/Genetic Toxicology and Environmental Mutagenesis*, 745 (1), 92–103.

Aruoja, V., Dubourguier, H.-C., Kasemets, K., and Kahru, A., 2009. Toxicity of nanoparticles of CuO, ZnO and TiO2 to microalgae Pseudokirchneriella subcapitata. *The Science of the Total Environment*, 407 (4), 1461–1468.

Ashburner, M., Ball, C.A., Blake, J.A., Botstein, D., Butler, H., Cherry, J.M., Davis, A.P., Dolinski, K., Dwight, S.S., Eppig, J.T., Harris, M.A., Hill, D.P., Issel-Tarver, L., Kasarskis, A., Lewis, S., Matese, J.C., Richardson, J.E., Ringwald, M., Rubin, G.M., and Sherlock, G., 2000. Gene ontology: tool for the unification of biology. The Gene Ontology Consortium. *Nature Genetics*, 25 (1), 25–29.

Bachelet-Violette, L., Silva, A.K.A., Maire, M., Michel, A., Brinza, O., Ou, P., Ollivier, V., Nicoletti, A., Wilhelm, C., Letourneur, D., Ménager, C., and Chaubet, F., 2014. Strong and specific interaction of ultra small superparamagnetic iron oxide nanoparticles and human activated platelets mediated by fucoidan coating. *RSC Advances*, 4 (10), 4864–4871.

Baker, T.J., Tyler, C.R., and Galloway, T.S., 2014. Impacts of metal and metal oxide

nanoparticles on marine organisms. *Environmental Pollution*, 186, 257–271.

Baltaci, A.K. and Yuce, K., 2018. Zinc Transporter Proteins. *Neurochemical Research*, 43 (3), 517–530.

Bardou, P., Mariette, J., Escudié, F., Djemiel, C., and Klopp, C., 2014. jvenn: an interactive Venn diagram viewer. *BMC bioinformatics*, 15, 293.

Blinova, I., Ivask, A., Heinlaan, M., Mortimer, M., and Kahru, A., 2010. Ecotoxicity of nanoparticles of CuO and ZnO in natural water. *Environmental Pollution*, 158 (1), 41–47.

Bondarenko, O., Juganson, K., Ivask, A., Kasemets, K., Mortimer, M., and Kahru, A., 2013. Toxicity of Ag, CuO and ZnO nanoparticles to selected environmentally relevant test organisms and mammalian cells in vitro: a critical review. *Archives of Toxicology*, 87 (7), 1181–1200.

Brayner, R., Couté, A., Livage, J., Perrette, C., and Sicard, C., 2011. Micro-algal biosensors. *Analytical and Bioanalytical Chemistry*, 401 (2), 581–597.

Bundschuh, M., Filser, J., Lüderwald, S., McKee, M.S., Metreveli, G., Schaumann, G.E., Schulz, R., and Wagner, S., 2018. Nanoparticles in the environment: where do we come from, where do we go to? *Environmental Sciences Europe*, 30 (1).

Canesi, L. and Corsi, I., 2016. Effects of nanomaterials on marine invertebrates. *The Science of the Total Environment*, 565, 933–940.

Carballeira, C., Ramos-Gómez, J., Martín-Díaz, L., and DelValls, T.A., 2012. Identification of specific malformations of sea urchin larvae for toxicity assessment: application to marine pisciculture effluents. *Marine Environmental Research*, 77, 12–22.

Châtel, A. and Mouneyrac, C., 2017. Signaling pathways involved in metal-based nanomaterial toxicity towards aquatic organisms. *Comparative Biochemistry and Physiology Part C: Toxicology & Pharmacology*, 196, 61–70.

Chen, F., Xiao, Z., Yue, L., Wang, J., Feng, Y., Zhu, X., Wang, Z., and Xing, B., 2019. Algae

response to engineered nanoparticles: current understanding, mechanisms and implications. *Environmental Science: Nano*, 6 (4), 1026–1042.

Chiu, M.-H., Khan, Z.A., Garcia, S.G., Le, A.D., Kagiri, A., Ramos, J., Tsai, S.-M., Drobenaire, H.W., Santschi, P.H., Quigg, A., and Chin, W.-C., 2017. Effect of Engineered Nanoparticles on Exopolymeric Substances Release from Marine Phytoplankton. *Nanoscale Research Letters*, 12 (1), 620.

Coffman, J.A. and Davidson, E.H., 2001. Oral–Aboral Axis Specification in the Sea Urchin Embryo. *Developmental Biology*, 230 (1), 18–28.

Covian-Nares, J.F., Smith, R.M., and Vogel, S.S., 2008. Two independent forms of endocytosis maintain embryonic cell surface homeostasis during early development. *Developmental Biology*, 316 (1), 135–148.

Crawford, B.J. and Burke, R.D., 2004. TEM and SEM Methods. *In*: *Methods in Cell Biology*. Academic Press, 411–441.

Cuvelier, M.L., Guo, J., Ortiz, A.C., van Baren, M.J., Tariq, M.A., Partensky, F., and Worden, A.Z., 2017. Responses of the picoprasinophyte Micromonas commoda to light and ultraviolet stress. *PloS One*, 12 (3), e0172135.

Derelle, E., Ferraz, C., Escande, M.-L., Eychenié, S., Cooke, R., Piganeau, G., Desdevises, Y., Bellec, L., Moreau, H., and Grimsley, N., 2008. Life-cycle and genome of OtV5, a large DNA virus of the pelagic marine unicellular green alga Ostreococcus tauri. *PloS One*, 3 (5), e2250.

Exbrayat, J.-M., Moudilou, E.N., and Lapied, E., 2015. Harmful Effects of Nanoparticles on Animals [online]. *Journal of Nanotechnology*. Available from: https://www.hindawi.com/journals/jnt/2015/861092/ [Accessed 12 Mar 2020].

Fairbairn, E.A., Keller, A.A., Mädler, L., Zhou, D., Pokhrel, S., and Cherr, G.N., 2011. Metal oxide nanomaterials in seawater: linking physicochemical characteristics with biological

response in sea urchin development. *Journal of Hazardous Materials*, 192 (3), 1565–1571.

Franklin, N.M., Rogers, N.J., Apte, S.C., Batley, G.E., Gadd, G.E., and Casey, P.S., 2007. Comparative toxicity of nanoparticulate ZnO, bulk ZnO, and ZnCl2 to a freshwater microalga (Pseudokirchneriella subcapitata): the importance of particle solubility. *Environmental Science & Technology*, 41 (24), 8484–8490.

Gambardella, C., Ferrando, S., Gatti, A.M., Cataldi, E., Ramoino, P., Aluigi, M.G., Faimali, M., Diaspro, A., and Falugi, C., 2016. Review: Morphofunctional and biochemical markers of stress in sea urchin life stages exposed to engineered nanoparticles. *Environmental Toxicology*, 31 (11), 1552–1562.

George, S., Pokhrel, S., Xia, T., Gilbert, B., Ji, Z., Schowalter, M., Rosenauer, A., Damoiseaux, R., Bradley, K.A., Mädler, L., and Nel, A.E., 2010. Use of a rapid cytotoxicity screening approach to engineer a safer zinc oxide nanoparticle through iron doping. *ACS nano*, 4 (1), 15–29.

Gottschalk, F., Lassen, C., Kjoelholt, J., Christensen, F., and Nowack, B., 2015. Modeling flows and concentrations of nine engineered nanomaterials in the Danish environment. *International Journal of Environmental Research and Public Health*, 12 (5), 5581–5602.

Gottschalk, F., Sun, T., and Nowack, B., 2013. Environmental concentrations of engineered nanomaterials: review of modeling and analytical studies. *Environmental Pollution (Barking, Essex: 1987)*, 181, 287–300.

Guillard, R.R.L. and Hargraves, P.E., 1993. Stichochrysis immobilis is a diatom, not a chrysophyte. *Phycologia*, 32 (3), 234–236.

Hanssen, K.Ø., Andersen, J.H., Stiberg, T., Engh, R.A., Svenson, J., Genevière, A.-M., and Hansen, E., 2012. Antitumoral and mechanistic studies of ianthelline isolated from the Arctic sponge Stryphnus fortis. *Anticancer Research*, 32 (10), 4287–4297.

Heinlaan, M., Ivask, A., Blinova, I., Dubourguier, H.-C., and Kahru, A., 2008. Toxicity of

nanosized and bulk ZnO, CuO and TiO2 to bacteria Vibrio fischeri and crustaceans Daphnia magna and Thamnocephalus platyurus. *Chemosphere*, 71 (7), 1308–1316.

Hou, J., Wu, Y., Li, X., Wei, B., Li, S., and Wang, X., 2018. Toxic effects of different types of zinc oxide nanoparticles on algae, plants, invertebrates, vertebrates and microorganisms. *Chemosphere*, 193, 852–860.

Huang, K., Diener, D.R., Mitchell, A., Pazour, G.J., Witman, G.B., and Rosenbaum, J.L., 2007. Function and dynamics of PKD2 in Chlamydomonas reinhardtii flagella. *The Journal of Cell Biology*, 179 (3), 501–514.

Kadar, E., Simmance, F., Martin, O., Voulvoulis, N., Widdicombe, S., Mitov, S., Lead, J.R., and Readman, J.W., 2010. The influence of engineered Fe2O3 nanoparticles and soluble (FeCl3) iron on the developmental toxicity caused by CO2-induced seawater acidification. *Environmental Pollution*, 158 (12), 3490–3497.

Kanehisa, M., Araki, M., Goto, S., Hattori, M., Hirakawa, M., Itoh, M., Katayama, T., Kawashima, S., Okuda, S., Tokimatsu, T., and Yamanishi, Y., 2008. KEGG for linking genomes to life and the environment. *Nucleic Acids Research*, 36 (Database issue), D480-484.

Kanehisa, M., Goto, S., Hattori, M., Aoki-Kinoshita, K.F., Itoh, M., Kawashima, S., Katayama, T., Araki, M., and Hirakawa, M., 2006. From genomics to chemical genomics: new developments in KEGG. *Nucleic Acids Research*, 34 (Database issue), D354-357.

Keller, A.A. and Lazareva, A., 2014. Predicted Releases of Engineered Nanomaterials: From Global to Regional to Local. *Environmental Science & Technology Letters*, 1 (1), 65–70.

Keller, A.A., Wang, H., Zhou, D., Lenihan, H.S., Cherr, G., Cardinale, B.J., Miller, R., and Ji, Z., 2010. Stability and aggregation of metal oxide nanoparticles in natural aqueous matrices. *Environmental Science & Technology*, 44 (6), 1962–1967.

Kim, R.-O., Choi, J.S., Kim, B.-C., and Kim, W.-K., 2017. Comparative Analysis of

Transcriptional Profile Changes in Larval Zebrafish Exposed to Zinc Oxide Nanoparticles and Zinc Sulfate. *Bulletin of Environmental Contamination and Toxicology*, 98 (2), 183–189.

Klimova, E.M., Bozhkov, A.I., Bychenko, E.A., Lavinskaya, E.V., Zholobak, N.M., and Korobov, A.M., 2019. Characteristics of the response of the microalga (Dunaliella viridis) to cerium compounds in culture. *Biosystems Diversity*, 27 (2), 142–147.

Landa, P., Vankova, R., Andrlova, J., Hodek, J., Marsik, P., Storchova, H., White, J.C., and Vanek, T., 2012. Nanoparticle-specific changes in Arabidopsis thaliana gene expression after exposure to ZnO, TiO2, and fullerene soot. *Journal of Hazardous Materials*, 241–242, 55–62.

Lead, J.R., Batley, G.E., Alvarez, P.J.J., Croteau, M.-N., Handy, R.D., McLaughlin, M.J., Judy, J.D., and Schirmer, K., 2018. Nanomaterials in the environment: Behavior, fate, bioavailability, and effects-An updated review. *Environmental Toxicology and Chemistry*, 37 (8), 2029–2063.

Levy, M., Luciani, N., Alloyeau, D., Elgrabli, D., Deveaux, V., Pechoux, C., Chat, S., Wang, G., Vats, N., Gendron, F., Factor, C., Lotersztajn, S., Luciani, A., Wilhelm, C., and Gazeau, F., 2011. Long term in vivo biotransformation of iron oxide nanoparticles. *Biomaterials*, 32 (16), 3988–3999.

Lewinski, N., Colvin, V., and Drezek, R., 2008. Cytotoxicity of Nanoparticles. *Small*, 4 (1), 26–49.

Ma, H., Bertsch, P.M., Glenn, T.C., Kabengi, N.J., and Williams, P.L., 2009. Toxicity of manufactured zinc oxide nanoparticles in the nematode Caenorhabditis elegans. *Environmental Toxicology and Chemistry*, 28 (6), 1324–1330.

Ma, H., Williams, P.L., and Diamond, S.A., 2013. Ecotoxicity of manufactured ZnO nanoparticles – A review. *Environmental Pollution*, 172, 76–85.

Magro, M., Sinigaglia, G., Nodari, L., Tucek, J., Polakova, K., Marusak, Z., Cardillo, S., Salviulo, G., Russo, U., Stevanato, R., Zboril, R., and Vianello, F., 2012. Charge binding of

rhodamine derivative to OH− stabilized nanomaghemite: Universal nanocarrier for construction of magnetofluorescent biosensors. *Acta Biomaterialia*, 8 (6), 2068–2076.

Majedi, S.M., Lee, H.K., and Kelly, B.C., 2012. Chemometric Analytical Approach for the Cloud Point Extraction and Inductively Coupled Plasma Mass Spectrometric Determination of Zinc Oxide Nanoparticles in Water Samples. *Analytical Chemistry*, 84 (15), 6546–6552.

Manzo, S., Miglietta, M.L., Rametta, G., Buono, S., and Di Francia, G., 2013. Embryotoxicity and spermiotoxicity of nanosized ZnO for Mediterranean sea urchin Paracentrotus lividus. *Journal of Hazardous Materials*, 254–255, 1–9.

Marcus, M., Karni, M., Baranes, K., Levy, I., Alon, N., Margel, S., and Shefi, O., 2016. Iron oxide nanoparticles for neuronal cell applications: uptake study and magnetic manipulations. *Journal of Nanobiotechnology*, 14.

Marisa, I., Matozzo, V., Munari, M., Binelli, A., Parolini, M., Martucci, A., Franceschinis, E., Brianese, N., and Marin, M.G., 2016. In vivo exposure of the marine clam Ruditapes philippinarum to zinc oxide nanoparticles: responses in gills, digestive gland and haemolymph. *Environmental Science and Pollution Research International*, 23 (15), 15275–15293.

Marrone, V., Piscopo, M., Romano, G., Ianora, A., Palumbo, A., and Costantini, M., 2012. Defensome against toxic diatom aldehydes in the sea urchin Paracentrotus lividus. *PloS One*, 7 (2), e31750.

Massart, R., 1981. Preparation of aqueous magnetic liquids in alkaline and acidic media. *IEEE Transactions on Magnetics*, 17 (2), 1247–1248.

Migliaccio, O., Castellano, I., Romano, G., and Palumbo, A., 2014. Stress response to cadmium and manganese in Paracentrotus lividus developing embryos is mediated by nitric oxide. *Aquatic Toxicology (Amsterdam, Netherlands)*, 156, 125–134.

Miller, R.J., Lenihan, H.S., Muller, E.B., Tseng, N., Hanna, S.K., and Keller, A.A., 2010.

Impacts of Metal Oxide Nanoparticles on Marine Phytoplankton. *Environmental Science & Technology*, 44 (19), 7329–7334.

Mitchell, D.R., 2007. The evolution of eukaryotic cilia and flagella as motile and sensory organelles. *Advances in Experimental Medicine and Biology*, 607, 130–140.

Montané, M.-H. and Kloppstech, K., 2000. The family of light-harvesting-related proteins (LHCs, ELIPs, HLIPs): was the harvesting of light their primary function? *Gene*, 258 (1), 1–8.

Montané, M.-H., Petzold, B., and Kloppstech, K., 1999. Formation of early-light-inducible-protein complexes and status of xanthophyll levels under high light and cold stress in barley (Hordeum vulgare L.). *Planta*, 208 (4), 519–527.

von Moos, N. and Slaveykova, V.I., 2014. Oxidative stress induced by inorganic nanoparticles in bacteria and aquatic microalgae--state of the art and knowledge gaps. *Nanotoxicology*, 8 (6), 605–630.

Morelli, E., Gabellieri, E., Bonomini, A., Tognotti, D., Grassi, G., and Corsi, I., 2018. TiO2 nanoparticles in seawater: Aggregation and interactions with the green alga Dunaliella tertiolecta. *Ecotoxicology and Environmental Safety*, 148, 184–193.

Mukherjee, K. and Acharya, K., 2018. Toxicological Effect of Metal Oxide Nanoparticles on Soil and Aquatic Habitats. *Archives of Environmental Contamination and Toxicology*, 75 (2), 175–186.

Oliviero, M., Schiavo, S., Rametta, G., Miglietta, M.L., and Manzo, S., 2017. Different sizes of ZnO diversely affected the cytogenesis of the sea urchin Paracentrotus lividus. *The Science of the Total Environment*, 607–608, 176–183.

Park, H.-G. and Yeo, M.-K., 2015. Comparison of gene expression patterns from zebrafish embryos between pure silver nanomaterial and mixed silver nanomaterial containing cells of Hydra magnipapillata. *Molecular & Cellular Toxicology*, 11 (3), 307–314.

Piticharoenphun, S., Šiller, L., Lemloh, M.-L., Salome, M., Cotte, M., Kaulich, B., Gianoncelli, A., Mendis, B.G., Bangert, U., Poolton, N.R.J., Horrocks, B.R., Brümmer, F., and Medaković, D., 2012. Agglomeration of Silver Nanoparticles in Sea Urchin. *International Journal of Environmental Pollution and Remediation*.

Polak, N., Read, D.S., Jurkschat, K., Matzke, M., Kelly, F.J., Spurgeon, D.J., and Stürzenbaum, S.R., 2014. Metalloproteins and phytochelatin synthase may confer protection against zinc oxide nanoparticle induced toxicity in Caenorhabditis elegans. *Comparative Biochemistry and Physiology Part C: Toxicology & Pharmacology*, 160, 75–85.

Qian, H., Zhu, K., Lu, H., Lavoie, M., Chen, S., Zhou, Z., Deng, Z., Chen, J., and Fu, Z., 2016. Contrasting silver nanoparticle toxicity and detoxification strategies in Microcystis aeruginosa and Chlorella vulgaris: New insights from proteomic and physiological analyses. *Science of The Total Environment*, 572, 1213–1221.

Quigg, A., Chin, W.-C., Chen, C.-S., Zhang, S., Jiang, Y., Miao, A.-J., Schwehr, K.A., Xu, C., and Santschi, P.H., 2013. Direct and Indirect Toxic Effects of Engineered Nanoparticles on Algae: Role of Natural Organic Matter. *ACS Sustainable Chemistry & Engineering*, 1 (7), 686–702.

Ragusa, M.A., Costa, S., Cuttitta, A., Gianguzza, F., and Nicosia, A., 2017. Coexposure to sulfamethoxazole and cadmium impairs development and attenuates transcriptional response in sea urchin embryo. *Chemosphere*, 180, 275–284.

Robinson, M.D., McCarthy, D.J., and Smyth, G.K., 2010. edgeR: a Bioconductor package for differential expression analysis of digital gene expression data. *Bioinformatics*, 26 (1), 139–140.

Roccheri, M.C., Agnello, M., Bonaventura, R., and Matranga, V., 2004. Cadmium induces the expression of specific stress proteins in sea urchin embryos. *Biochemical and Biophysical Research Communications*, 321 (1), 80–87.

Rocha, T.L., Gomes, T., Sousa, V.S., Mestre, N.C., and Bebianno, M.J., 2015. Ecotoxicological impact of engineered nanomaterials in bivalve molluscs: An overview. *Marine Environmental Research*, 111, 74–88.

Roger, J., Pons, J.N., Massart, R., Halbreich, A., and Bacri, J.C., 1999. Some biomedical applications of ferrofluids. *The European Physical Journal Applied Physics*, 5 (3), 321–325.

Russo, R., Bonaventura, R., and Matranga, V., 2014. Time- and dose-dependent gene expression in sea urchin embryos exposed to UVB. *Marine Environmental Research*, 93, 85–92.

Satori, C.P., Kostal, V., and Arriaga, E.A., 2011. Individual organelle pH determinations of magnetically-enriched endocytic organelles via laser-induced fluorescence detection. *Analytical chemistry*, 83 (19), 7331–7339.

Scheibe, R., 2004. Malate valves to balance cellular energy supply. *Physiologia Plantarum*, 120 (1), 21–26.

Silva, B.F. da, Pérez, S., Gardinalli, P., Singhal, R.K., Mozeto, A.A., and Barceló, D., 2011. Analytical chemistry of metallic nanoparticles in natural environments. *TrAC Trends in Analytical Chemistry*, 30 (3), 528–540.

Singhal, R.K., Preetha, J., Karpe, R., Tirumalesh, K., Kumar, S.C., and Hegde, A.G., 2006. The use of ultra filtration in trace metal speciation studies in sea water. *Environment International*, 32 (2), 224–228.

Su, G., Zhang, X., Giesy, J.P., Musarrat, J., Saquib, Q., Alkhedhairy, A.A., and Yu, H., 2015. Comparison on the molecular response profiles between nano zinc oxide (ZnO) particles and free zinc ion using a genome-wide toxicogenomics approach. *Environmental Science and Pollution Research*, 22 (22), 17434–17442.

Sun, Z. and Ettensohn, C.A., 2017. TGF-β sensu stricto signaling regulates skeletal morphogenesis in the sea urchin embryo. *Developmental Biology*, 421 (2), 149–160.

Torres-Duarte, C., Adeleye, A.S., Pokhrel, S., Mädler, L., Keller, A.A., and Cherr, G.N., 2016. Developmental effects of two different copper oxide nanomaterials in sea urchin (Lytechinus pictus) embryos. *Nanotoxicology*, 10 (6), 671–679.

Torres-Duarte, C., Ramos-Torres, K.M., Rahimoff, R., and Cherr, G.N., 2017. Stage specific effects of soluble copper and copper oxide nanoparticles during sea urchin embryo development and their relation to intracellular copper uptake. *Aquatic Toxicology (Amsterdam, Netherlands)*, 189, 134–141.

Trask, B.J., van den Engh, G.J., and Elgershuizen, J.H., 1982. Analysis of phytoplankton by flow cytometry. *Cytometry*, 2 (4), 258–264.

Tsiokas, L., 2009. Function and regulation of TRPP2 at the plasma membrane. *American Journal of Physiology. Renal Physiology*, 297 (1), F1-9.

Tualla, I.P.B. and Bitacura, J.G., 2016. Effects of Cadmium and Zinc on the Gamete Viability, Fertilization, and Embryonic Development of Tripneustes gratilla (Linnaeus). *Scientifica*, 2016, 8175213.

Valdiglesias, V., Fernández-Bertólez, N., Kiliç, G., Costa, C., Costa, S., Fraga, S., Bessa, M.J., Pásaro, E., Teixeira, J.P., and Laffon, B., 2016. Are iron oxide nanoparticles safe? Current knowledge and future perspectives. *Journal of Trace Elements in Medicine and Biology*, 38, 53–63.

Wong, S.W.Y., Leung, P.T.Y., Djurišić, A.B., and Leung, K.M.Y., 2010. Toxicities of nano zinc oxide to five marine organisms: influences of aggregate size and ion solubility. *Analytical and Bioanalytical Chemistry*, 396 (2), 609–618.

Worden, A.Z., Lee, J.-H., Mock, T., Rouzé, P., Simmons, M.P., Aerts, A.L., Allen, A.E., Cuvelier, M.L., Derelle, E., Everett, M.V., Foulon, E., Grimwood, J., Gundlach, H., Henrissat, B., Napoli, C., McDonald, S.M., Parker, M.S., Rombauts, S., Salamov, A., Von Dassow, P., Badger, J.H., Coutinho, P.M., Demir, E., Dubchak, I., Gentemann, C., Eikrem,

W., Gready, J.E., John, U., Lanier, W., Lindquist, E.A., Lucas, S., Mayer, K.F.X., Moreau, H., Not, F., Otillar, R., Panaud, O., Pangilinan, J., Paulsen, I., Piegu, B., Poliakov, A., Robbens, S., Schmutz, J., Toulza, E., Wyss, T., Zelensky, A., Zhou, K., Armbrust, E.V., Bhattacharya, D., Goodenough, U.W., Van de Peer, Y., and Grigoriev, I.V., 2009. Green evolution and dynamic adaptations revealed by genomes of the marine picoeukaryotes Micromonas. *Science (New York, N.Y.)*, 324 (5924), 268–272.

Wu, B., Torres-Duarte, C., Cole, B.J., and Cherr, G.N., 2015. Copper oxide and zinc oxide nanomaterials act as inhibitors of multidrug resistance transport in sea urchin embryos: their role as chemosensitizers. *Environmental Science & Technology*, 49 (9), 5760–5770.

Xia, T., Kovochich, M., Liong, M., Mädler, L., Gilbert, B., Shi, H., Yeh, J.I., Zink, J.I., and Nel, A.E., 2008. Comparison of the Mechanism of Toxicity of Zinc Oxide and Cerium Oxide Nanoparticles Based on Dissolution and Oxidative Stress Properties. *ACS Nano*, 2 (10), 2121–2134.

Yung, M.M.N., Wong, S.W.Y., Kwok, K.W.H., Liu, F.Z., Leung, Y.H., Chan, W.T., Li, X.Y., Djurišić, A.B., and Leung, K.M.Y., 2015. Salinity-dependent toxicities of zinc oxide nanoparticles to the marine diatom Thalassiosira pseudonana. *Aquatic Toxicology*, 165, 31–40.

Zhao, X., Wang, S., Wu, Y., You, H., and Lv, L., 2013. Acute ZnO nanoparticles exposure induces developmental toxicity, oxidative stress and DNA damage in embryo-larval zebrafish. *Aquatic Toxicology*, 136–137, 49–59.

Zhou, C., Carotenuto, Y., Vitiello, V., Wu, C., Zhang, J., and Buttino, I., 2018. De novo transcriptome assembly and differential gene expression analysis of the calanoid copepod Acartia tonsa exposed to nickel nanoparticles. *Chemosphere*, 209, 163–172.

Figure captions:

Figure 1. TEM analysis of γ-Fe_2O_3 (A) and ZnO (B) ENPs dispersed in NFSW. Evolution of the hydrodynamic diameter (C) of Fe_2O_3 ENPs dispersed in NFSW, [Fe] = 5.10^{-3} mol/L at 20°C. Dotted lines represent the sedimentation threshold. TEM analysis of γ-Fe_2O_3 ENP dispersed in L1 algal culture medium along the time (D-F). Scale bar 100 nm.

Figure 2. Developmental abnormalities of *P. lividus* embryos observed 48h post fertilization. Embryos were maintained in NFSW (A), the control condition, or exposed to Fe_2O_3 ENPs (B) or $FeCl_3$ (C) at 5 10^{-5} mol/L and ZnO ENPs (D) or $ZnSO_4$ (E) at 1 10^{-5} mol/L. Dose response to zinc derivative exposure (F). These results are representative of three independent experiments. Scale bar 100 μm.

Figure 3. Internalization of Fe_2O_3 ENPs into sea urchin embryos observed by TEM 24h p.f.. Embryos were incubated with Fe_2O_3 ENPs at 1 10^{-4} mol/L. ENPs are accumulated in vesicles in the cytoplasm of embryonic cells. Cells were observed at low (A) or high magnification (B,C). A: Blastocoel (Bl) and ectodermal cells (Ec) of the embryo are indicated. B: a white arrow indicates an internal vesicle containing ENPs. C: a cytoplasmic vesicle (V) containing ENPs is indicated close to the outer cell membrane. D: Identification of Fe_2O_3 ENPs in internal vesicle was confirmed by TEM with Elemental Analysis. The red arrow in the top spectrum indicate the iron peak. The bottom spectrum correspond to the control zone.

Figure 4. Venn diagrams showing common and specific responses of *P. lividus* embryos exposed to metal ENPs or corresponding ions (5.0 10^{-5} mol/L [Fe], 2.8 10^{-3} g/L, for Fe_2O_3 ENPs and 10^{-5} mol/L [Zn], 6.5 10^{-4} g/L, for ZnO ENPs). Up-regulated genes (A) ; down-regulated

genes (B). The “size of each list” correspond to the number of significantly up- or down-regulated genes (FDR threshold = 1%) in response to each treatment.

Figure 5. Time course of *M. commoda* culture growth in response to increasing concentrations of Fe_2O_3 (A) or ZnO ENPs (B). Cells were counted by flow cytometry. IC50 assay for the analysis of half-maximal inhibitory concentration of Fe_2O_3 (C) or ZnO ENPs (D) in *M. commoda* cell culture 48h post treatment. Algae were incubated without (control) or with ENPs using [Fe] or [Zn] concentration from 10^{-7} to 10^{-4} mol/L. Data were analyzed with Graphpad-Prism7. These results are representative of three independent experiments.

Figure 6. TEM images of microalgae exposed to Fe_2O_3 ENPs (5 10^{-5} mol/L). ENPs appeared in contact with cell surface membranes. C: Chloroplaste, F: Flagellum, M: Mitochondria, N: Nucleus, S: Starch granule. In Fig D, E and F, cells were dividing. Scale bar 100 nm.

Figure 7. Venn diagrams showing common and specific responses of *M. commoda* exposed to metal ENPs or corresponding ions (3 10^{-5} mol/L [Fe],1.7 10^{-3} g/L, for Fe_2O_3 ENPs and 10^{-5} mol/L [Zn], 6.5 10^{-4} g/L, for ZnO ENPs). Up-regulated genes (A) ; down-regulated genes (B). The “size of each list” correspond to the number of significantly up- or down-regulated genes (FDR threshold = 1%) in response to each treatment.

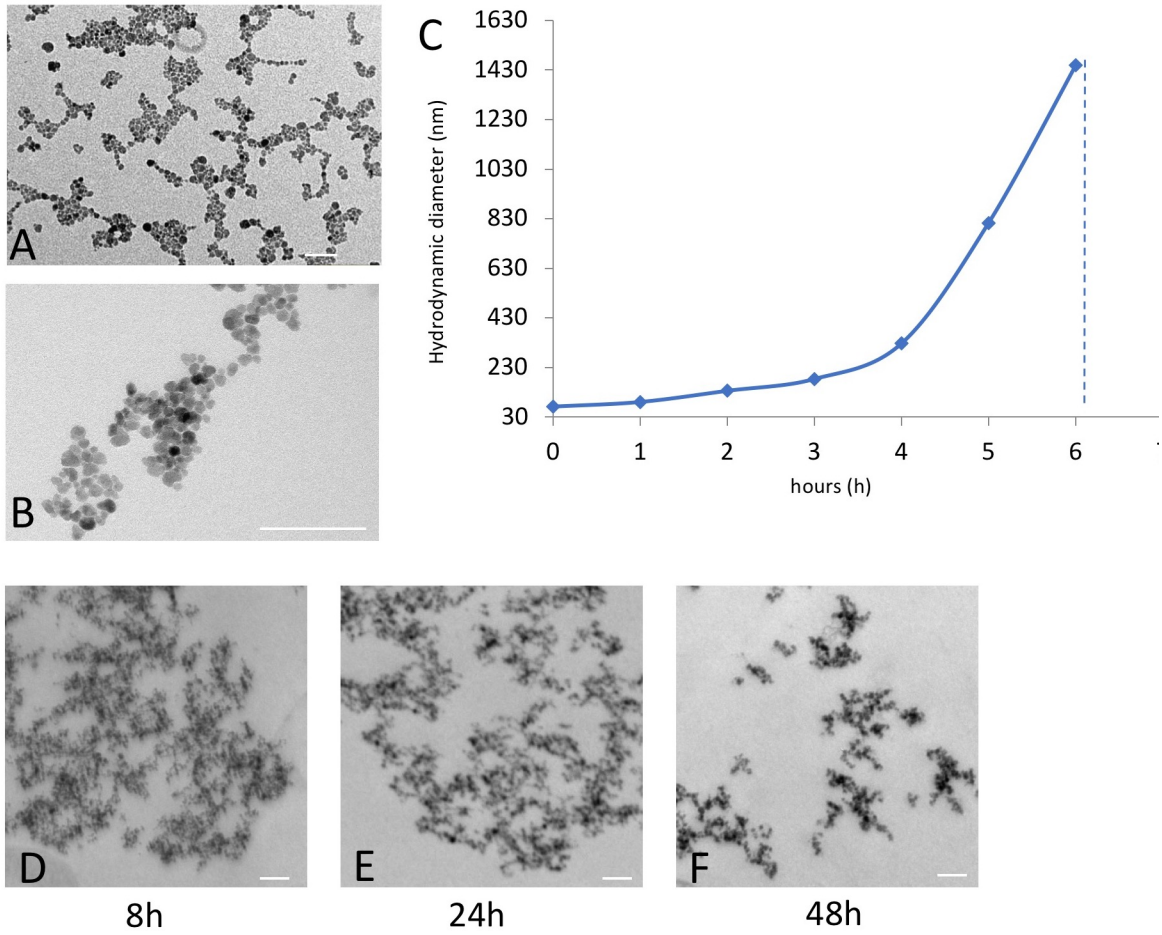
A
B
C
1630
1430
1230
1030
830
630
430
230
30
Hydrodynamic diameter (nm)
0
1
2
3
4
5
6
hours (h)
D
E
F
8h
24h
48h

Figure 1

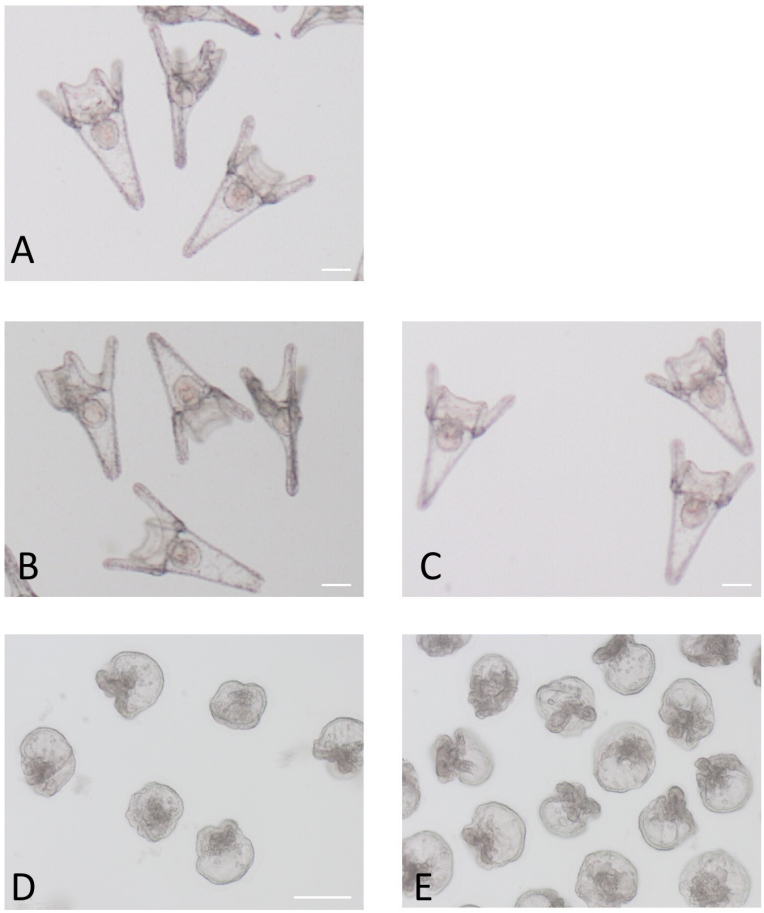
A
B
C
D
E

F

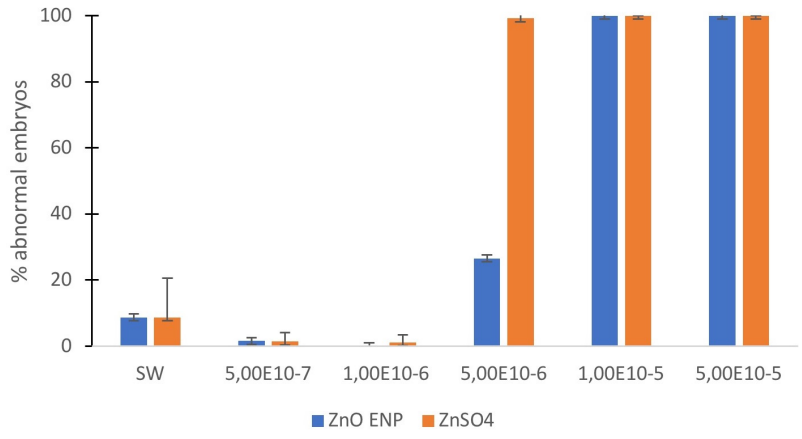
100
80
60
40
20
0
% abnormal embryos
SW
5,00E10-7
1,00E10-6
5,00E10-6
1,00E10-5
5,00E10-5
ZnO ENP
ZnSO4

Figure 2

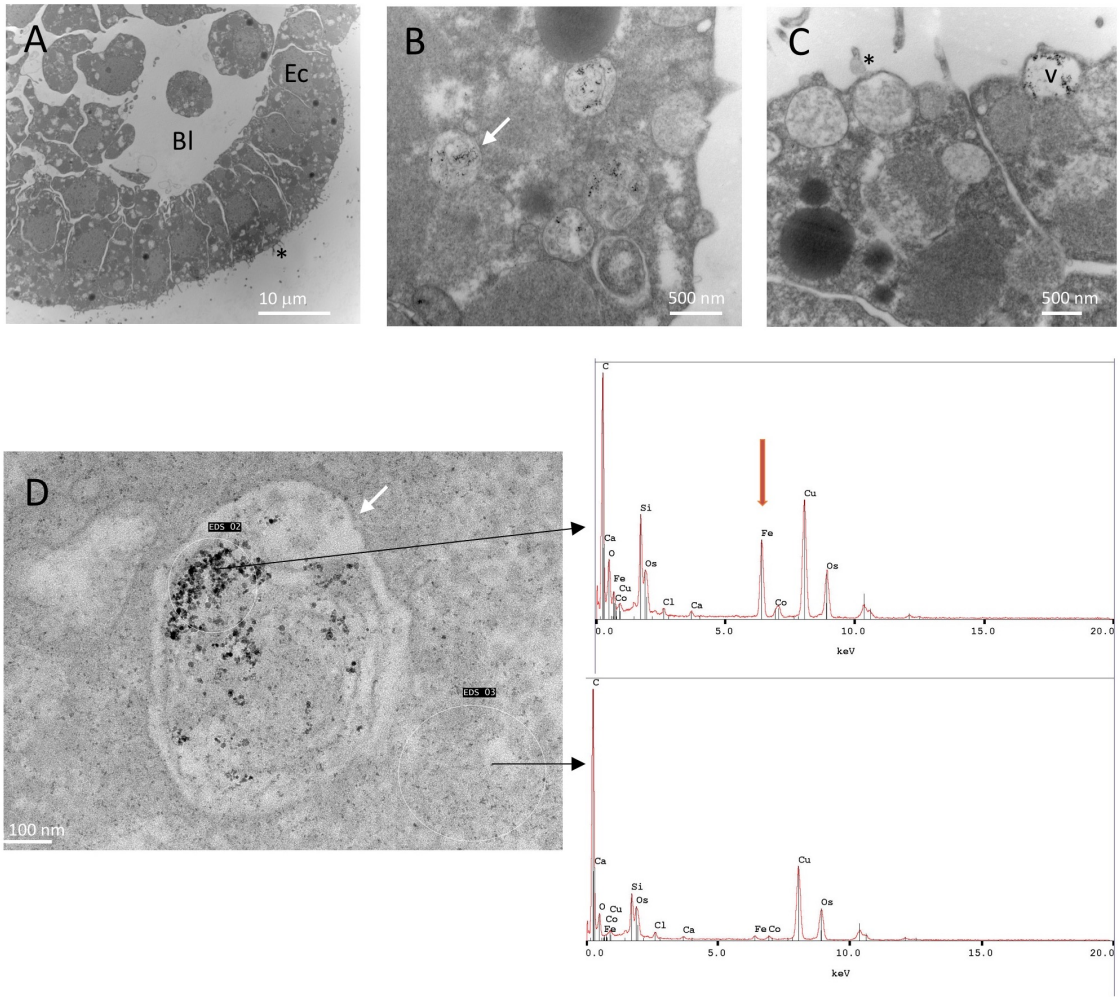
A
Ec
Bl
*
10 µm
B
500 nm
C
*
V
500 nm
D
EDS_02
EDS_03
100 nm
C
Ca
O
Si
Fe
Cu
Co
Os
Cl
Ca
Fe
Co
Cu
Os
0.0
5.0
10.0
15.0
20.0
keV
C
Ca
O
Cu
Co
Fe
Si
Os
Cl
Ca
Fe Co
Cu
Os
0.0
5.0
10.0
15.0
20.0
keV

Figure 3

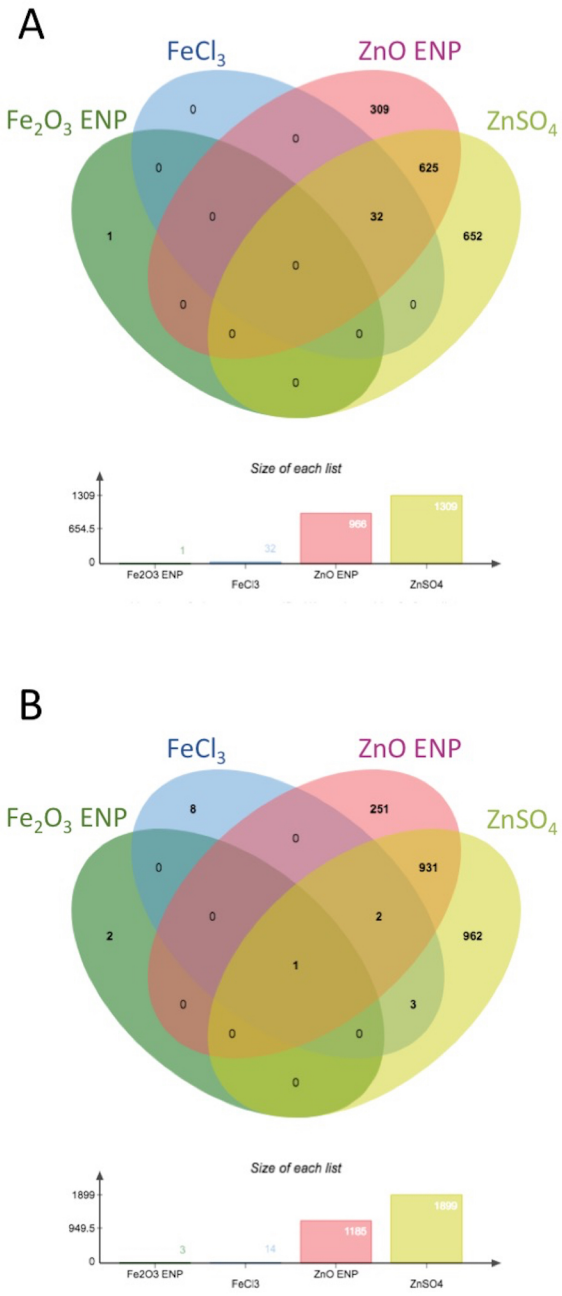
A
FeCl3
ZnO ENP
Fe2O3 ENP
ZnSO4
0
309
0
0
625
0
32
1
652
0
0
0
0
0
0
Size of each list
1309
654.5
0
1
32
966
1309
Fe2O3 ENP
FeCl3
ZnO ENP
ZnSO4
B
FeCl3
ZnO ENP
Fe2O3 ENP
ZnSO4
8
251
0
0
931
0
2
2
962
1
0
3
0
0
0
Size of each list
1899
949.5
0
3
14
1185
1899
Fe2O3 ENP
FeCl3
ZnO ENP
ZnSO4

Figure 4

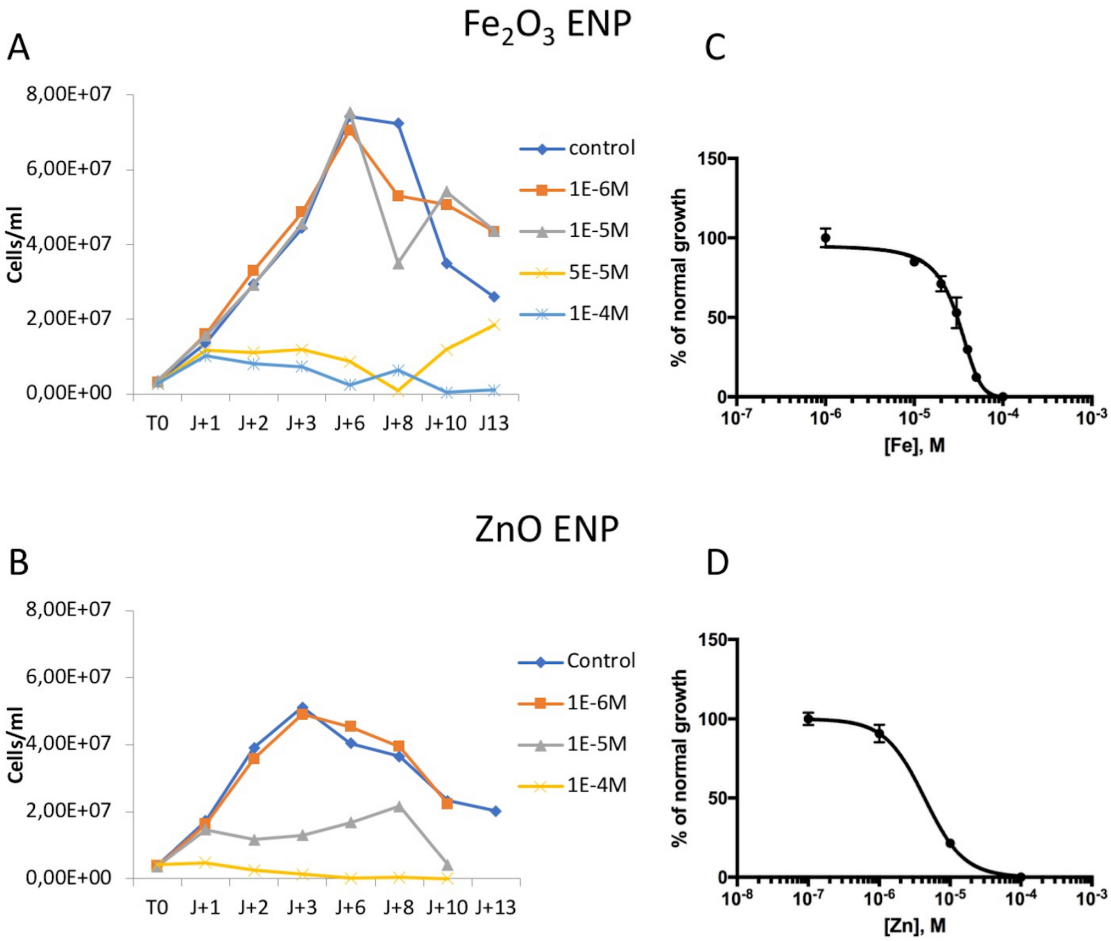
A
Fe2O3 ENP
8,00E+07
6,00E+07
4,00E+07
2,00E+07
0,00E+00
Cells/ml
T0 J+1 J+2 J+3 J+6 J+8 J+10 J13
control
1E-6M
1E-5M
5E-5M
1E-4M
C
% of normal growth
150
100
50
0
10-7 10-6 10-5 10-4 10-3
[Fe], M
B
ZnO ENP
8,00E+07
6,00E+07
4,00E+07
2,00E+07
0,00E+00
Cells/ml
T0 J+1 J+2 J+3 J+6 J+8 J+10 J13
Control
1E-6M
1E-5M
1E-4M
D
% of normal growth
150
100
50
0
10-8 10-7 10-6 10-5 10-4 10-3
[Zn], M

Figure 5

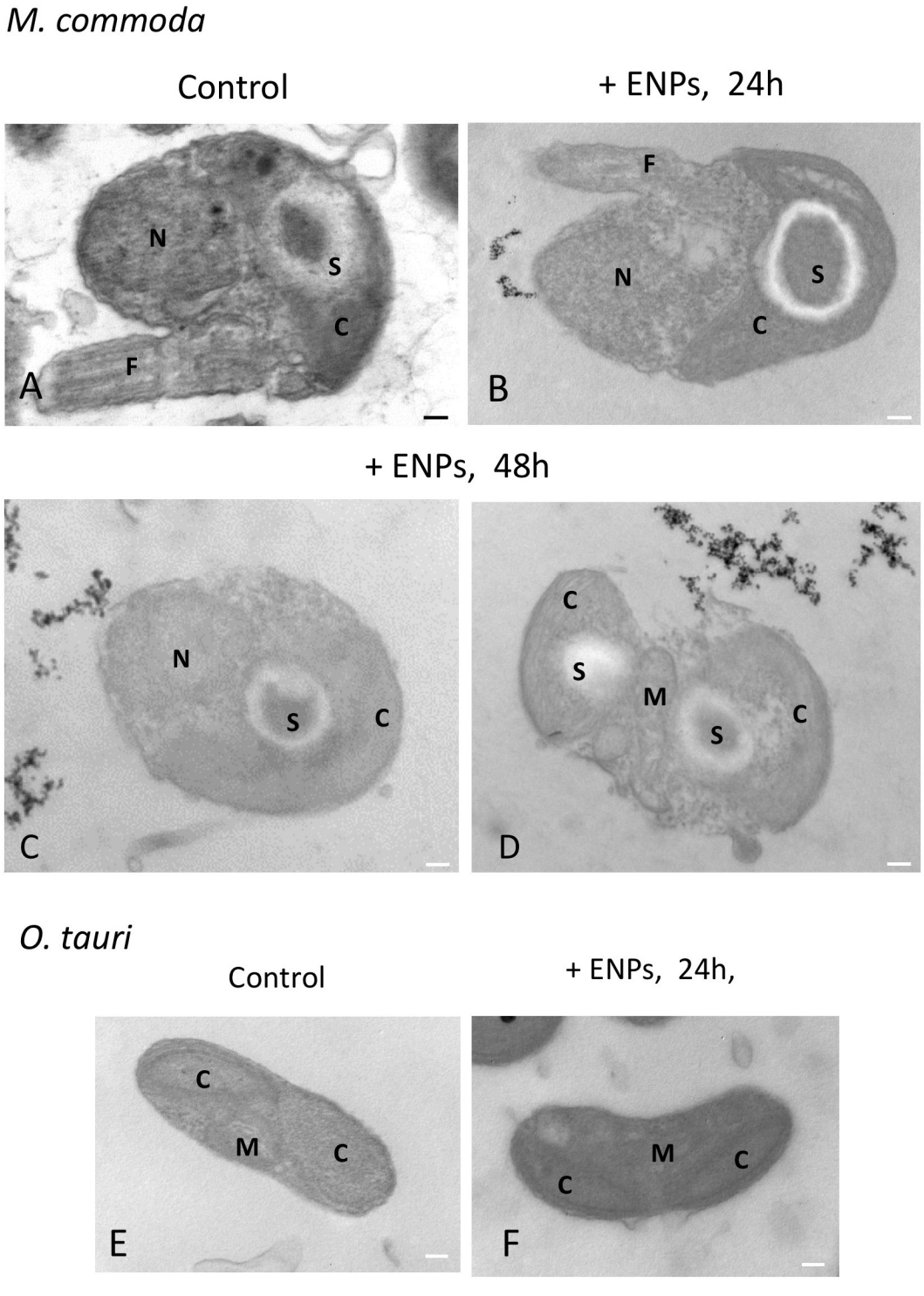
M. commoda
Control
+ ENPs, 24h
N
S
C
F
A
F
N
S
C
B
+ ENPs, 48h
N
S
C
C
S
M
S
C
C
D
O. tauri
Control
+ ENPs, 24h,
C
M
C
E
M
C
C
F

Figure 6

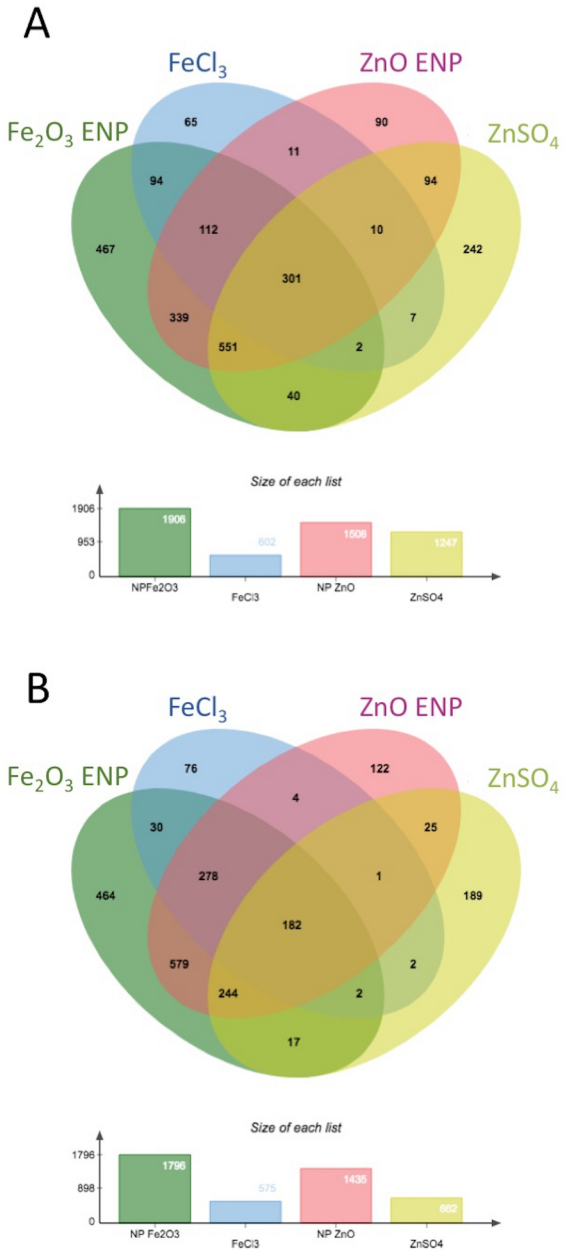
A
FeCl3
ZnO ENP
Fe2O3 ENP
ZnSO4
65
90
11
94
94
112
10
467
242
301
339
7
551
2
40
Size of each list
1906
953
0
1906
602
1508
1247
NPFe2O3
FeCl3
NP ZnO
ZnSO4
B
FeCl3
ZnO ENP
Fe2O3 ENP
ZnSO4
76
122
4
30
25
278
1
464
189
182
579
2
244
2
17
Size of each list
1796
898
0
1796
575
1435
662
NP Fe2O3
FeCl3
NP ZnO
ZnSO4

Figure 7